

Site-Directed Mutagenesis of UDP-Galactopyranose Mutase Reveals a Critical Role for the Active-Site, Conserved Arginine Residues[†]

Jennifer M. Chad,[‡] Karunan Partha Sarathy,[‡] Todd D. Gruber,[§] Eshwari Addala,[‡] Laura L. Kiessling,^{§,∇} and David A. R. Sanders^{*,‡}

Department of Chemistry, University of Saskatchewan, Saskatoon, SK, Canada, S7N 5C9, and Departments of Biochemistry and of Chemistry, University of Wisconsin—Madison, Madison, Wisconsin 53706-1396

Received February 8, 2007; Revised Manuscript Received April 3, 2007

ABSTRACT: The flavoenzyme UDP-galactopyranose mutase (UGM) is a mediator of cell wall biosynthesis in many pathogenic microorganisms. UGM catalyzes a unique ring contraction reaction that results in the conversion of UDP-galactopyranose (UDP-Galp) to UDP-galactofuranose (UDP-Galf). UDP-Galf is an essential precursor to the galactofuranose residues found in many different cell wall glycoconjugates. Due to the important consequences of UGM catalysis, structural and biochemical studies are needed to elucidate the mechanism and identify the key residues involved. Here, we report the results of site-directed mutagenesis studies on the absolutely conserved residues in the putative active site cleft. By generating variants of the UGM from *Klebsiella pneumoniae*, we have identified two arginine residues that play critical catalytic roles (alanine substitution abolishes detectable activity). These residues also have a profound effect on the binding of a fluorescent UDP derivative that inhibits UGM, suggesting that the Arg variants are defective in their ability to bind substrate. One of the residues, Arg280, is located in the putative active site, but, surprisingly, the structural studies conducted to date suggest that Arg174 is not. Molecular dynamics simulations indicate that closed UGM conformations can be accessed in which this residue contacts the pyrophosphoryl group of the UDP-Gal substrates. These results provide strong evidence that the mobile loop, noted in all the reported crystal structures, must move in order for UGM to bind its UDP-galactose substrate.

The cell wall of pathogenic microorganisms has been a target for antimicrobial drugs for many years. Since this highly complex and species-specific structure has a number of components not found in humans and other higher eukaryotes, the biosynthesis of the cell wall and its individual components continues to be an attractive target for development of novel antimicrobial drugs. One such component is D-galactofuranose (Galf^f), the 5-membered-ring form of galactose. Galf residues are found as components of the cell walls of pathogenic bacteria such as *Escherichia coli*, *Klebsiella pneumoniae*, and *Mycobacterium tuberculosis* (1–5). It is also found in the cell walls of fungi such as *Aspergillus fumigatus* (6–8), and in cell-surface structures of protozoa such as *Trypanosoma cruzi* (9) and *Leishmania* species (10–13). *M. tuberculosis* is the causative agent of

tuberculosis (TB), a disease declared a global health emergency by the World Health Organization (WHO) in 1993 that kills around 3 million people annually (more than AIDS and malaria combined) (14). *M. tuberculosis* has a unique cell wall, consisting of an external mycolic acid layer connected to the peptidoglycan through an arabinogalactan layer. Galf is a vital component of this arabinogalactan complex (15, 16). The active precursor to Galf is UDP- α -D-galactofuranose (UDP-Galf), which is converted from UDP- α -D-galactopyranose (UDP-Galp) by the flavoenzyme UDP-galactopyranose mutase (UGM). It has been shown by McNeil and co-workers that UGM is essential for the viability of mycobacteria (15). Although a number of studies have been carried out on UGM, the mechanism of ring contraction is still not fully understood. Understanding this mechanism can facilitate the development of novel anti-TB therapies.

In the past few years, the structures of UGM from *E. coli*, *K. pneumoniae*, and *M. tuberculosis* have been determined by X-ray crystallography (17, 18). These structures all superimpose on each other with a C α rmsd under 1.20 Å over the entire monomer structure. The structures reveal that UGM is a homodimer and member of the mixed α/β protein class. The proposed active site cleft lies at the interface of two domains: one is the structurally conserved flavin-binding domain (domain 1), and the other is a novel 5 helical bundle (domain 2). The previous structural studies have identified several conserved residues that project into the active site

[†] This work was supported by an NSERC Discovery Grant (RG-PIN250238-02) to D.A.R.S. and an NIH Research Grant (RO1 AI64596) to L.L.K.; T.D.G. was supported by the NIH Biotechnology Training Program (T32 GM008349), J.M.C. was supported by an NSERC USRA, and E.A. was supported by the BMST Graduate Scholarship program.

* Address correspondence to this author: Department of Chemistry, University of Saskatchewan, Saskatoon, Saskatchewan, Canada S7N 5C9. Tel: 306-966-6788. Fax: 306-966-4730. E-mail: david.sanders@usask.ca.

[‡] University of Saskatchewan.

[§] Department of Biochemistry, University of Wisconsin—Madison.

[∇] Department of Chemistry, University of Wisconsin—Madison.

¹ Abbreviations: Galf, galactofuranose; Galp, galactopyranose; UMP, uridine 5'-monophosphate; UDP-Galp, UDP-D-galactopyranose; UDP-Galf, UDP-D-galactofuranose; FAD, flavin adenine dinucleotide; wt, wild-type.

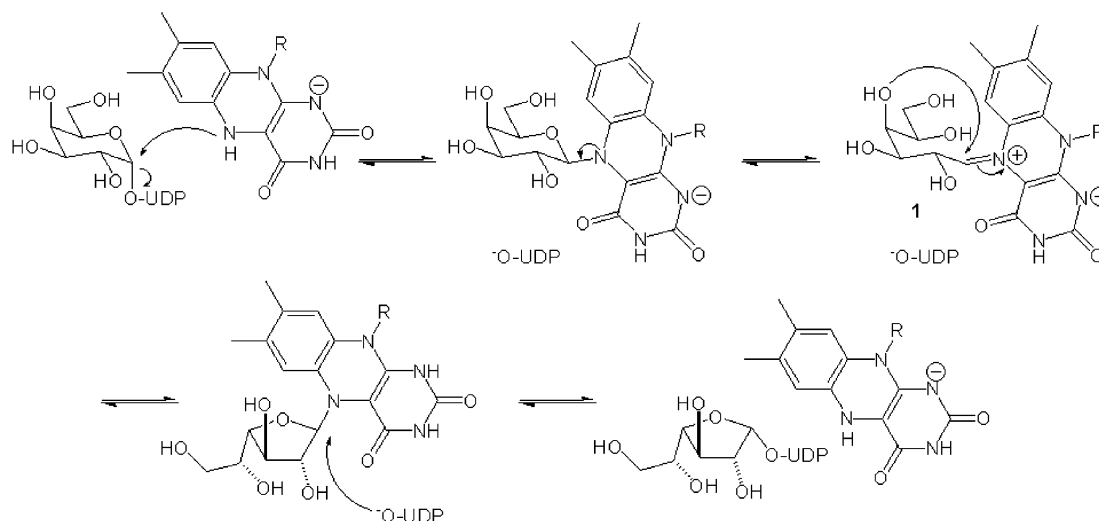


FIGURE 1: Proposed mechanism for the conversion of UDP-Galp to UDP-Galf catalyzed by UGM. The iminium ion intermediate (1) is formed through nucleophilic attack by the N5 of the reduced flavin and subsequent ring opening of the galactose adduct. A similar set of transformations generates UDP-Galp from UDP-Galf.

and therefore are poised to participate in binding and catalysis (18). To date there is no crystal structure of UGM complexed with substrates or inhibitors. All attempts to cocrystallize or soak substrates into the protein crystals have been unsuccessful (17–19): either no crystals or crystals of the apoenzyme were obtained. Recently, an STD-NMR/molecular modeling study was reported that offers insight into the binding mode of UDP-Galp with UGM (20). In that study, a model for the binding of UDP-Galp was put forth; key features include an interaction of the uridine moiety with the conserved tryptophan residue and the sugar ring in position to form a bond with the flavin isoalloxazine ring.

A number of different roles have been proposed for the flavin, including nucleophilic attack (21), single electron transfer (19), hydride transfer (5, 22), charge stabilization, and a structural role (22, 23). Mechanisms that have no role for the flavin have been put forward, including one involving a 1,4-anhydro- β -D-galactopyranose intermediate. Bicyclic compounds have been synthesized, but these neither inhibit nor serve as substrates for UGM (24, 25). Indeed, mechanistic studies implicate a catalytic role for the flavin cofactor. Specifically, a reduced flavin is required for catalytic activity; the oxidized flavoenzyme is inactive (18, 19, 21). The Kiessling group has proposed an alternative mechanism involving a flavin-galactose iminium intermediate (Figure 1), and they have demonstrated that the reduction product of this intermediate can be generated using NaCNBH₄ (21). A variety of additional mechanisms have been proposed for UGM (19, 21–23, 26, 27); however the current data best support the nucleophilic mechanism (Figure 1).

Despite the wealth of structural and biochemical data, questions remain about the mechanism and the role of the flavin. We reasoned that site-directed mutagenesis could provide insight into both of these issues. We carried out a mutational analysis of the absolutely conserved residues in UGM that are believed to play roles in substrate binding/catalytic activity of this important enzyme. We have demonstrated that while all of the mutations have some effect on activity, thus far, there are only two that have been found to be critical: the substitution of either of two key arginines results in a completely inactive enzyme. The key role of one

of these arginine residues (Arg280) can be rationalized by the crystal structures determined to date. It is located in proximity to the negatively charged pyrophosphate group. In contrast, the other arginine (Arg174) side chain is oriented away from the active site. This residue is located on a flexible loop at the “mouth” of the active site. For it to play a role in catalysis, this loop must rearrange upon substrate binding. This rearrangement is consistent with previously reported studies on STD-NMR binding (20).

EXPERIMENTAL PROCEDURES

Cloning. The wild-type *K. pneumoniae* mutase gene and the mutant proteins W160A, Y155F, Y185F, Y346F, and Y314F were generated as described previously (18). The gene products all carry a C-terminal His₆-tag. Site-directed mutagenesis for the rest of the mutant enzymes was carried out using the QuikChange XL kit (Stratagene, USA) and confirmed by DNA sequencing. The primers used were as follows:

R174A 5'-GCATCTATTCTTAAAGCTCTTCCTGTTCG
5'-CGAACAGGAAGAGCTTTAAGAATAGATGC
R280A 5'-GTGCCCTATACTGCTATCACTGAACATAAATATTTTC
5'-GAAAAATATTTATGTTTCAGTGATAGCAGTATAGGGCAC
E301A 5'-CTCTGTTATAAAGCGTATAGCCGTGC
5'-GCACGGCTATGCTTTATAACAGAG
D351A 5'-CCGTTACCTTGCTATGATGTGACC
5'-GGTCACATCATAGCAAGGTAACGG
H60A 5'-GTTTATGGACCCGCTATTTCCATACTGAC
5'-GTCAGTATGGAAAATAGCGGGTCCATAAAC

Protein Purification. The proteins were overproduced and purified following a similar protocol to the one described previously (18). *E. coli* Rosetta (Novagen) competent cells were transformed with the plasmids. The cells were grown in 1 L of LB broth (in Fernbach flasks) at 37 °C to an OD₆₀₀ of 0.6. The flasks were then cooled, and induction was initiated by IPTG addition (final concentration of 0.4 mM).

The cells were incubated for a further 3 h at 25 °C. The cells were pelleted and stored at -80 °C until purified.

The cell pellets were thawed and resuspended in 100 mM potassium phosphate buffer (pH 8.0), 2 mM AEBSF (4-(2-aminoethyl)benzenesulfonyl fluoride hydrochloride), 0.5 mM EDTA, 20 µg/mL lysozyme, and 20 µg/mL DNase I (buffer B). The cells were further lysed by sonication. The cell debris was removed by centrifugation 30 min at 18 K rpm. The supernatant was then treated with 10% ammonium sulfate (AmSO₄) (w/v) and allowed to spin at 4 °C for 30 min. The solution was then spun for 30 min at 18 K to remove any additional precipitate. The supernatant was then loaded onto a MC50 POROS column (10 × 100 mm) (Applied Biosystems), precharged with 50 mM CuCl₂ and pre-equilibrated with 50 mM phosphate buffer (pH 8.0), 300 mM NaCl (buffer B), and 0.5 mM imidazole. The bound protein was eluted with a gradient of 0.5 mM to 100 mM imidazole in buffer B. The elution was monitored at 280 and 450 nm; the fractions corresponding to the 450 nm peak were collected, pooled, and concentrated to approximately 10 mL. This solution was then brought to 40% AmSO₄ (w/v) for application to a HP20 POROS column (10 × 100 mL) (Applied Biosystems) pre-equilibrated with 50 mM potassium phosphate buffer (pH 8.0), 40% AmSO₄ (w/v). The column was eluted with a gradient of 40% AmSO₄ to 0% AmSO₄ (in potassium phosphate, pH 8.0). The elution was monitored at 280 and 450 nm, and the fractions corresponding to the 450 nm peak were collected, pooled, and dialyzed vs 50 mM Tris-HCl, pH 7.5 for 4 changes overnight.

After dialysis, the protein was concentrated using an Amicon Ultraconcentrator. The concentration was determined by the method of Bradford (28), and the samples were flash-frozen in small aliquots (20 µL) in liquid nitrogen and stored at -80 °C as reported previously (18, 29).

Synthesis of UDP-Galf. UDP-Galf was synthesized and purified as described previously (30). The product was stored dried as a solid at -20 °C. Under these conditions, UDP-Galf is stable over extended periods (>6 months).

Circular Dichroism. All circular dichroism (CD) spectra for the wild type and the mutants of UGM were collected on a Pi-Star 180 spectrometer (Applied Photophysics, Leatherhead, U.K.) using a quartz cuvette with 0.01 cm path length over a far-UV wavelength range of 180–260 nm. The system was purged with N₂ (8–10 L/min) for 15–20 min. Protein samples were prepared in 10 mM phosphate buffer (pH 8.0). The concentration of each protein sample was maintained at 1 mg/mL. Data were collected every 0.5 nm and were the average of 10 repeat shots. In all cases, baseline scans of aqueous buffer were subtracted from the experimental readings. The results were expressed in units of delta epsilon and plotted versus the wavelength.

Enzyme Kinetic Assays. Enzyme assays were performed in a similar manner to earlier reported protocols (21, 22, 29, 31). The reactions were carried out in 100 mM MOPS buffer (pH 8.0), with fresh 20 mM sodium dithionite. The final volume of each reaction mixture was 30 µL. Initially, the enzyme concentration was adjusted for each different mutant to give a reasonable conversion (20–40%) within 2–3 min at 100 µM concentration (for example, wt UGM was used at a final concentration of 0.4 µM). Subsequent reactions, with varying substrate concentrations (5 µM to 5 mM) were carried out with the same enzyme concentration for all

reactions. The time of each reaction was adjusted to have % conversion values between 30% and 40%. The reactions were quenched by the addition of 50 µL of *n*-butanol. The aqueous layer was removed and injected onto a Waters HPLC system. The column used was a Gemini 5 µ (C-18) column (Phenomenex), pre-equilibrated with 50 mM triethylammonium acetate (pH 6.9), 1.5% acetonitrile. The samples were eluted isocratically and absorbance readings were carried out at 262 nm. The initial rate was then calculated from the initial concentration and the % conversion. Kinetic values were determined from nonlinear regression analysis using GraphPad Prism software.

For UGM variants R280A and R174A the assays were carried out using 500 µM protein concentration and 10 mM substrate for 60 min.

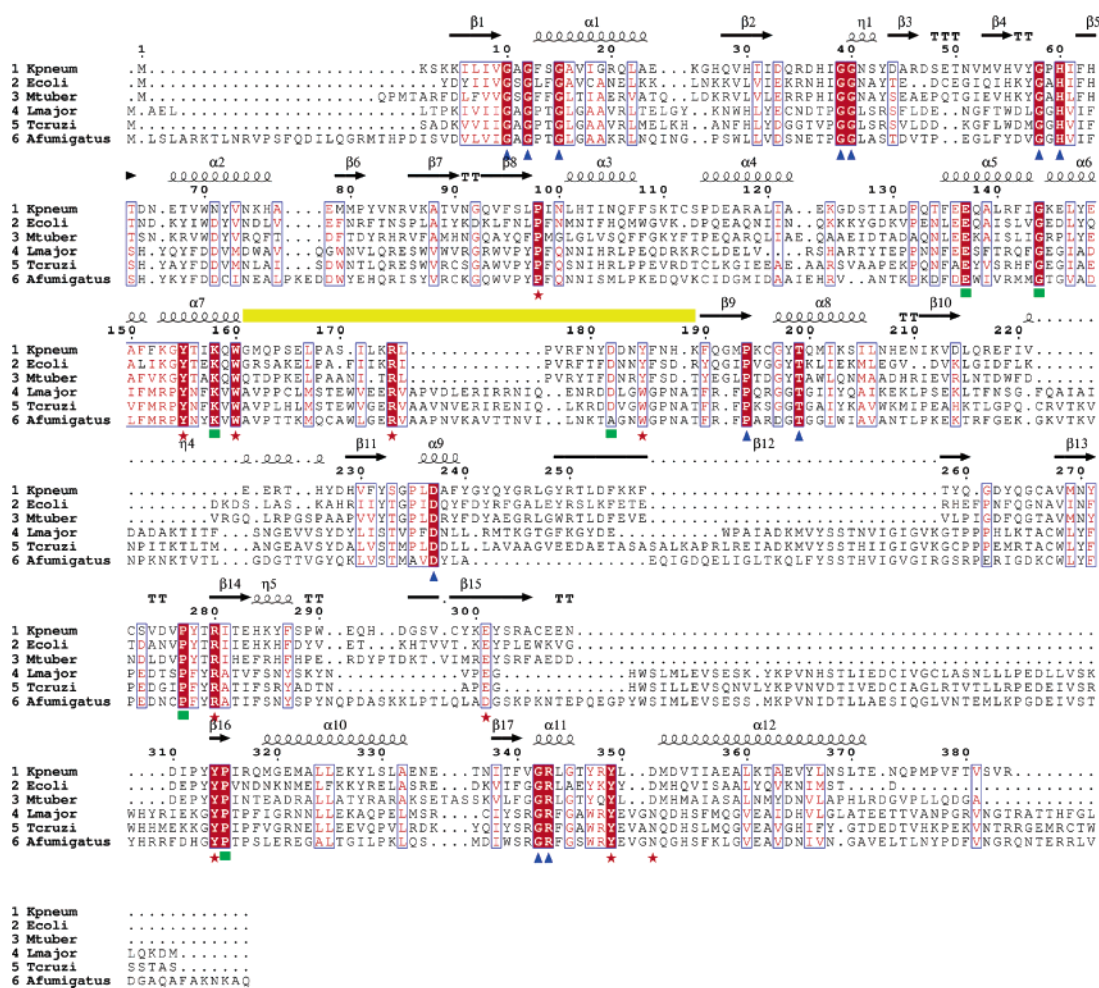
Dithionite Concentration Assay. Determination of the optimal sodium dithionite concentration was carried out using wt UGM (0.4 µM), with a fixed substrate concentration of 100 µM. The assay was carried out under the same conditions as described above, and the sodium dithionite concentration was varied. Each point was measured in triplicate.

Fluorescence Polarization Assay. Protein samples were dialyzed (10000 MWCO) against 2 L of 50 mM sodium phosphate pH 7.0 (2×, total dialysis time 16 h). Samples were concentrated using Centricon YM30 concentrators (Millipore, USA), and protein concentrations were determined using A₄₅₀ values ($\epsilon = 11300 \text{ M}^{-1} \text{ cm}^{-1}$). Binding assays were set up in a 384-well format as described previously (32). Protein concentration was varied from 1 nM to 10 µM in the presence of 15 nM UDP-fluorescein (UDP-F1). Millipolarization (mP) values were measured using a Perkin-Elmer Envision 2100 plate reader. Binding measurements were also recorded for wt UGM using the conjugate generated from the reaction fluorescein isothiocyanate with hexanolamine. This control probe, which lacks the UDP moiety but is otherwise identical to UDP-F1, provides a partial estimate of nonspecific signal relative to protein concentration. Control probe FP values were subtracted from corresponding UDP-F1 values to provide the final, normalized values (Figure 5). Data were fit to $y = (a - d)/(1 + (x/c)^{-b}) + d$ where a = maximum FP signal, b = slope, c = apparent K_d value, and d = minimum FP signal, using Kaleidagraph software (Synergy Software, USA).

Energy Minimization Calculations. An energy minimized model for UGM/UDP-Galp was developed with the InsightII/Discover software package (Accelrys Inc., San Diego, CA). The starting coordinates were from the model derived in a previous work (20), based on the 2.4 Å structure of *E. coli* UGM (18). Arginine 170 (*E. coli* sequence), which corresponds to Arg174 in *K. pneumoniae*, was constrained to be within 4 Å of the β -phosphate of the UDP-Galp substrate. This model was subjected to Simp_Min_Dyn calculations with 5000 steps of energy minimization with the derivative set to 0.05. The dynamics calculations were conducted for 100 ps duration with 1 fs step, and snapshots were collected every 0.5 ps. The dielectric constant was set to 1, and a nonperiodic boundary condition with NVT ensemble was defined. The average structure from the ensemble was collected and subjected to further 1000 steps of energy minimization with the convergence criteria set to 0.05.

Substrate Docking Study. Docking of UDP-Galp into the modeled active site of UGM was performed following the

A)



B)

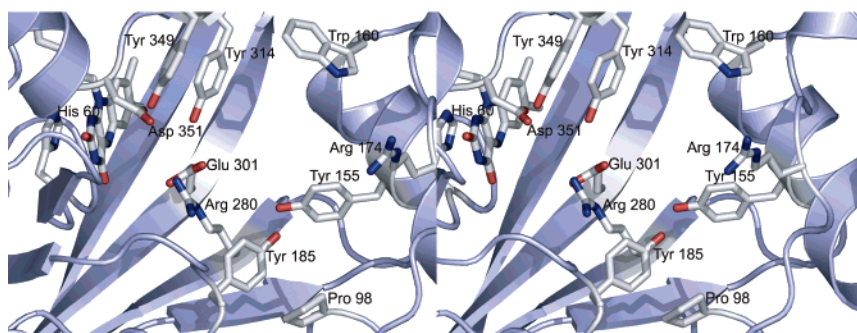


FIGURE 2: Choice of residues for site-directed mutagenesis: identification of conserved residues in active site. (A) Sequence alignment generated from 14 bacterial UGMs and 4 eukaryotic UGMs. Only 6 sequences are shown; however, to conserve space the sequence identity/similarity is based on the alignment of all sequences. The secondary structure shown above the sequences is based on the crystal structure of *K. pneumoniae* (PDB code: 2B17). Conserved residues found in the active site are marked with a red asterisk, blue triangles mark the location of conserved residues found in the flavin binding domain, and residues with unidentified function are marked with green squares. The mobile loop is indicated by the yellow bars. Alignment was carried out by T_{COFFEE} (34) and the figure generated using ESPrInt (44) (B) Stereodiagram of the active site of *K. pneumoniae* UGM showing the conserved residues. All molecular figures were generated using Pymol (DeLano Scientific).

procedure used previously (20). We again started from the structure of the complex derived above. All of the active torsion angles of UDP-Galp were allowed to be fully flexible during the docking experiment with AutoDock 3.05 (33). The grid maps were constructed using $70 \times 70 \times 70$ points, with grid point spacing of 0.375 \AA . The Lamarckian genetic

algorithm (LGA) was used with the default settings, and 25 LGA docking runs were performed.

Loop Movement Simulation. The molecular dynamics simulations were performed using the Discover_3 module within the InsightII software package (Accelrys Inc., San Diego, CA). The model of the open conformation of UGM

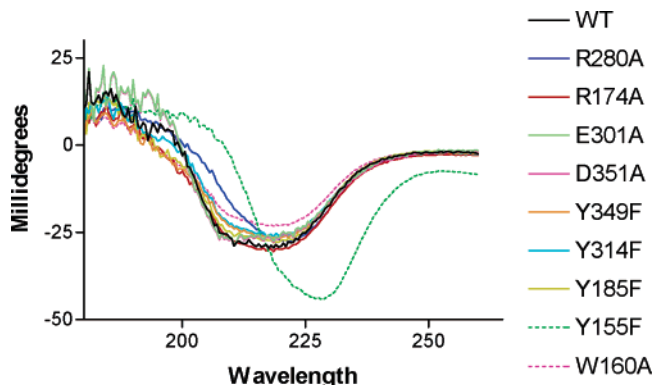


FIGURE 3: Circular dichroism spectra for wild-type UGM and active site mutants. The concentration of the protein was maintained at 1 mg/mL. In all cases, baseline scans of aqueous buffer were subtracted from the experimental readings. The reasons for the changes in the spectrum for Y155F are not known.

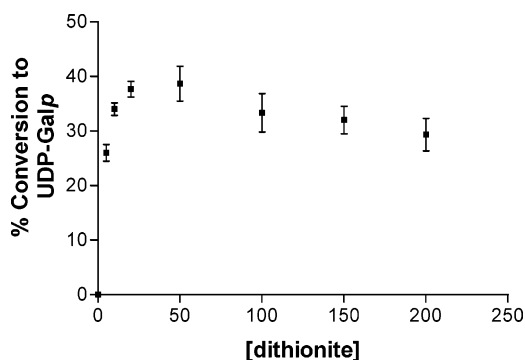


FIGURE 4: Effects of changing the concentration of sodium dithionite on the conversion of UDP-galactopyranose to UDP-galactofuranose by UGM. The reaction conditions (enzyme concentration, substrate concentration, time) were identical for each experiment with only the concentration of sodium dithionite changing. Each measurement was made 3 times.

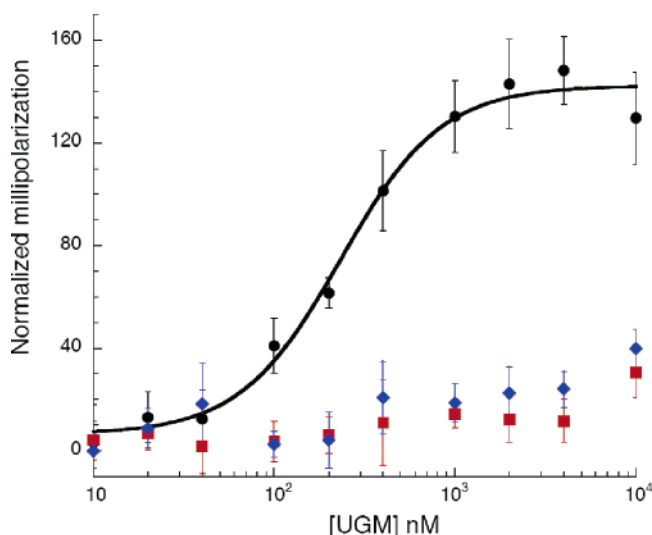


FIGURE 5: Fluorescence polarization binding assay of arginine variants. The K_d value for wt UGM (black) binding to the UDP-FI probe is 250 ± 70 nM. R174A (red) and R280A (blue) show no specific binding. At higher concentrations of UGM, increased nonspecific binding makes K_d value determination impossible.

was generated by using the B monomer of *E. coli* UGM and positioning UDP-Galp in the same orientation as it was modeled into monomer A (above and Yuan et al. (20)). The molecular dynamics simulation was carried out as described

Table 1: Sequence Numbers for Conserved Active Site Residues of UGM from *K. pneumoniae*, *E. coli*, and *M. tuberculosis*

<i>K. pneumoniae</i>	<i>E. coli</i>	<i>M. tuberculosis</i>
H60	H56	H65
Y155	Y151	Y161
W160	W156	W166
R174	R170	R180
Y185	Y181	Y191
R280	R278	R292
E301	E298	E315
Y314	Y311	E328
Y349	Y346	Y366
D351	D348	D368

above, except we did not constrain the distance between Arg170 and the β -phosphoryl group of UDP-Galp.

RESULTS AND DISCUSSION

Designing and Producing the UGM Variants. Our strategy was to generate variants of the UGM from *K. pneumoniae*. To identify residues of interest, we carried out a sequence alignment of 14 bacterial UGM homologues and 4 eukaryotic homologues using T-Coffee (34), which revealed a number of absolutely conserved residues (Figure 2A). Sequence identity between prokaryotic UGMs is approximately 40% and between eukaryotic UGMs is 45%, while the identity between the two sets is less than 20%. The conserved residues can be generally divided into two sets, those found in the flavin binding domain (noted with blue triangles in Figure 2A) and those positioned in or near the active site cleft (noted with red asterisks). The first set of residues is assumed to be critical for the binding and proper orientation of flavin, and is not the focus of this current study. There are several residues (Glu137, Gly144, Lys158, Asp182, Pro277, Pro315; green squares) that cannot be classified readily into either set, and are also beyond the scope of the current study. We focused our mutagenesis studies on active site residues that might contribute to catalysis (Table 1 and Figure 2B). Since studies have used the structures of *E. coli*, *K. pneumoniae*, and *M. tuberculosis* in their discussions, we include the sequence numbers from all three species in Table 1.

All of the protein variants chosen were produced and purified under similar conditions; the exception was H60A, which was produced as insoluble protein. As His60 appears to play a structural role in binding to the flavin isoalloxazine ring (17), the lack of solubility was likely caused by a lack of ability to bind flavin properly, resulting in improper protein folding.

Spectroscopic Analysis of UGM Variants. Wild-type UGM and all of the variants were analyzed by circular dichroism (Figure 3). With the exception of Y155F, all of the variants exhibited similar CD spectra, suggesting that they are folded correctly. There are discrepancies in the spectra for the R280A and Y155F variants. For the former, the changes are minor and likely inconsequential. The reason for the discrepancy in the Y155F variant is unknown; this protein exhibited decreased activity that may result from an increase in conformational flexibility. The results from UV spectroscopy show that all of these proteins (including R280A and Y155F) exhibit similar spectra between 300 and 600 nm (data not shown). These results indicate that the noncovalently

Table 2: Kinetic Values for the Conversion of UDP-Galactofuranose to UDP-Galactopyranose Catalyzed by UDP-Galactopyranose Mutase (UGM) from *K. pneumoniae*

protein	K_m (μM)	relative to wt	k_{cat} (min^{-1})	relative to wt	k_{cat}/K_m
wt	43 \pm 6	1.00	330 \pm 40	1.00	7.7×10^6
E301A	205 \pm 18	0.21	18 \pm 2	0.05	8.8×10^4
D351A	1002 \pm 284	0.04	8 \pm 2	0.02	8.0×10^3
W160A	2.53×10^6 ^a		n/a ^a		130 ^a
R280A	ND		ND		
R174A	ND		ND		
Y185F	386 \pm 92	0.11	78 \pm 14	0.24	2.0×10^5
Y155F	619 \pm 117	0.07	217 \pm 25	0.66	3.5×10^5
Y349F	739 \pm 63	0.06	103 \pm 16	0.31	1.4×10^5
Y314F	819 \pm 182	0.05	313 \pm 40	0.95	3.8×10^5

^a The K_m value for W160A was calculated assuming that the k_{cat} would be similar to wt.

bound flavin cofactor has been incorporated into all of the mutant proteins. Together, the spectroscopic data indicate that the protein variants are folded.

Enzyme Kinetics of UGM Variants. The protein variants of *K. pneumoniae* UGM created by site-directed mutagenesis were analyzed to determine the kinetic parameters. Since our HPLC assay is discontinuous, the maximum velocities were estimated from initial rates observed during the first 30–40% of reaction. To test the validity of this assumption, wild-type UGM was assayed at time points corresponding to 10%, 20%, 30%, 40%, and 50% reaction. The values for the 30% and 40% reaction time points gave the fastest rate with the most reproducible results (data not shown). Thus, this extent of reaction was used for all further experiments.

For each data point, the length of time for each substrate concentration was adjusted to give a 30% conversion of UDP-Galf to UDP-Galp. This time and actual turnover were used to approximate the initial velocity of the reaction. All of the mutants, except R280A and R174A, displayed sufficient turnover to calculate initial rates. The kinetic parameters for all the mutants and wild-type UGM are listed in Table 2.

We have determined the K_m and k_{cat} values of wt UGM to be 43 μM and 300 min^{-1} , respectively. These values are similar to the values previously reported for wild-type UGM ($K_m = 22 \mu\text{M}$ and $k_{\text{cat}} = 27 \text{ s}^{-1}$ for the conversion of UDP-Galf to UDP-Galp) (31, 35). There are several factors that might lead to these slight differences. The most likely explanation is that the proteins come from different clones and purification procedures and this is reflected in the kinetic parameters. It should be noted that wt UGM as purified by us has no detectable activity (until reduced by sodium dithionite), while others have reported residual activity from their purified samples (22, 23, 31, 36). We also considered the possibility that our protein was not fully reduced in our assays, and we used different dithionite concentrations to address this possibility (Figure 4). We found that maximum activity occurs at dithionite concentrations between 10 and 50 mM; consequently, UGM was fully reduced in our assays.

Active Site Tryptophan. The tryptophan residue located on the edge of the active site cleft is conserved in all species. This conservation is consistent with an important role for this residue. Indeed, the previous modeling studies predict that the uridine moiety forms a π -edge stacking interaction

with the tryptophan residue (20). In analyzing the activity of the W160A mutant, the curve of the initial rate vs substrate concentration remained linear and increased with increasing substrate concentration. To estimate the Michaelis–Menten kinetic parameters, the assumption was made that the V_{max} would be similar to that of wt UGM, and the curve was fit using a fixed value for V_{max} . The resulting estimated K_m is $2.53 \times 10^6 \mu\text{M}$. This is beyond the concentrations of substrate that can be achieved (the highest concentration that can be easily obtained is 10 mM). Our kinetic data indicate that removal of this residue has dramatic effects on the binding of substrate.

Conserved Tyrosines. The four conserved tyrosines have been suggested to be important for UGM activity (18). Analysis of UGM variant kinetics indicates that the major difference among them is an alteration in K_m ; all proteins display a 90% or greater decrease in binding. Conversely, these substitutions do not appear to have a large effect on the catalytic rates, indicating that these residues have little or no role in catalysis. A comparison of the sequences between prokaryotic and eukaryotic UGMs shows that Tyr185 is not absolutely conserved; the corresponding residue in eukaryotic UGMs is tryptophan (Figure 2A). The preservation of an aromatic residue at this position is consistent with a role in substrate binding but not catalysis (37). Interactions between aromatic amino acids and sugars have been previously observed in a number of sugar-binding proteins (37, 38). It has been suggested that tyrosine residues act as hydrogen bond donor/acceptors in stabilizing the binding of the sugar moiety (18). Though we cannot rule out some role in hydrogen bonding, it appears more likely that the aromaticity of the tyrosine residues contributes to substrate binding.

Aspartic Acid 351 and Glutamic Acid 301. Glu301 and Asp351 are both residues that point into the active site cleft; along with His63, they represent the only conserved residues in the prokaryotic enzymes that can easily function to stabilize a positive charge on the sugar moiety. In some UGM homologues, the residue corresponding to Glu301 is an aspartic acid; thus, this position could have a role either as a charge stabilizer or in hydrogen bond formation. Although Asp351 is absolutely conserved in prokaryotes, an asparagine is found in eukaryotes. This observation suggests that this side chain functions in hydrogen bond formation.

The E301A mutant has 5% of the activity of wt UGM, while still retaining most (21%) of the binding affinity. These data indicate that Glu301 may stabilize a charged intermediate (Figure 1) (19, 21–23). Previous modeling (20) positions this residue at a considerable distance from the bound UDP-Galp (6.7 Å from O-5 of the sugar). This location is consistent with the results of the kinetics experiments, which suggest that there must be a change in orientation of the intermediate with respect to the protein during catalysis.

The D351A substitution has large effects on both binding (4% of wt) and activity (2%). The model has Asp351 located 4.3 Å from 4-OH of the sugar. Since the corresponding residue in eukaryotes is an asparagine, it is reasonable that this residue engages in H-bonding interactions with the substrate. Some involvement in charge stabilization cannot be ruled out.

Conserved Arginine Residues. The UGM variants R174A and R280A are inactive. Even when the enzymatic reaction

is conducted using high enzyme concentrations (500 μM) and extended time periods (up to 1 h) with the highest substrate concentration available (10 mM), no turnover was observed. Importantly, the data indicate that both R174A and R280A are folded (Figure 3); thus, their lack of activity likely arises from the importance of these residues in catalysis or substrate binding.

When UDP-Galp is modeled in the active site of UGM, Arg280 can contact the phosphoryl groups of UDP-Galp (17, 20). This interaction could stabilize the UDP⁻ leaving group (27). Arg174 is also conserved across all known prokaryotic and eukaryotic UGMs (Figure 2A). In the structures solved to date, it is located on a flexible loop, positioned so that it is facing away from the active site cleft. Due to the flexibility of the loop, it is likely that Arg174 has the mobility to rotate so the guanidinium group is in the active site (see discussion below).

Substitution of Arginine Residues Decreases Substrate Binding Affinity. To determine whether the loss of activity observed for the Arg variants is due to a decrease in substrate binding affinity, effects on mechanism, or a combination of both, we used a fluorescence polarization assay to measure binding constants. This assay, developed for use in high throughput screens for UGM ligands, utilizes a UDP-fluorescein (UDP-FI) probe that has been shown to bind tightly and specifically to UGM from both *K. pneumoniae* and *M. tuberculosis* (32, 39). The ability of wt enzyme and the R174A and R280A (from *K. pneumoniae*, as above) variants to bind this probe was measured. The K_d value for UDP-FI binding to wt UGM was determined to be 250 ± 70 nM (Figure 5). The differences between the wt and mutant proteins had to be estimated because increases in millipolarization were observed as the concentration of enzyme was increased over several orders of magnitude; these increases were not saturable. It is apparent that the K_d values of R174A and R280A for the probe are increased greatly, and they are outside the range of the assay. The data indicate that these variants have binding constants that are increased by more than 2 orders of magnitude.

Structural Rationale for Role of Arg174: Role of Mobile Loop. The structures of UGM from *E. coli*, *K. pneumoniae*, and *M. tuberculosis*, which were determined by X-ray crystallography, show that UGM consists of three domains. Domain 1 consists of the structurally conserved flavin binding domain; domain 2 constitutes a novel 5 helical bundle; and domain 3 is a β -sheet “hinge” domain (Figure 6). The differences between the two monomers in *E. coli* structure indicate that the relationship of these domains can vary; domain 2 alters its position with respect to domain 1, with domain 3 serving as a molecular hinge. There are two flexible loops located at one edge of the cleft. Loop 2 (residues 157–185 in *E. coli*, see Figure 2A) forms one edge of the cleft, whereas loop 1 (residues 118–130 in *E. coli*) interacts with loop 2 (Figure 6). In the *E. coli* structure, two different conformations of the loops are present. Loop 2 in monomer A is in the “closed” conformation but in the “open” conformation in monomer B. The residues move up to 7 Å (C α position) between the two conformations. Both the *K. pneumoniae* and *M. tuberculosis* structures show a third possible orientation that results in up to 4 Å of additional movement in the loop (into an even more open conformation). In all of these structures the loop has temperature

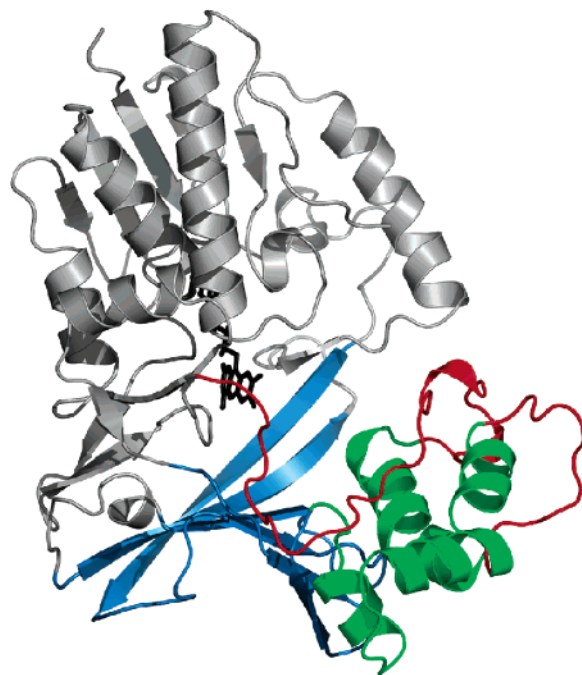


FIGURE 6: Ribbon diagram representation of a monomer of UGM. Representation of the *K. pneumoniae* monomer is depicting the flavin binding domain 1 (gray), domain 2 (green), and domain 3 (blue). The FAD group is shown as a stick model, colored black, while the two mobile loops are colored red. In the *K. pneumoniae* structure, these loops contain a short 3-10 helix.

factors that are 10–20 Å² higher than the rest of the protein (17, 18). Together these results indicate that this region of the protein is flexible.

Arg174 is located at the end of loop 2, with the side chain oriented away from the binding cleft (Figure 7A). In the structures solved to date, this residue (Arg174 or its equivalent) makes contacts within the crystal lattice (monomer A of *E. coli*, the *K. pneumoniae* monomer, monomer C of *M. tuberculosis* all form hydrogen bonds closer than 3.3 Å with residues from symmetry-related molecules). These observations suggest that the effects of the crystal lattice in the structures solved to date prevent UGM from adopting the “active” conformation of the protein. Alternatively, substrate binding may induce the active conformation. Since the current crystallization conditions all yield structures with some crystal contacts with the “open” conformation, UGM–substrate complexes may be difficult to crystallize because stabilizing lattice interactions are lost.

Molecular Dynamics Simulations of Loop Movement. To investigate our hypothesis that loop rearrangement allows Arg174 to make contacts with the substrate, we carried out several modeling studies. The initial study was conducted using the *E. coli* UGM/UDP-Galp model derived from STD-NMR and docking calculations (20). Using this model, we constrained the position of Arg170 (equivalent to Arg174 in *K. pneumoniae*), such that it was within 4 Å of the β -phosphoryl group of UDP-Galp, and performed energy minimization. The movement of the loop in this model (Figure 7B) results in a shift of the positions of 6 residues (greater than 1 Å movement of the C α positions of all the residues). Arg170 rotates 94° into the cleft and moves 3 Å (C α movement) toward the substrate. The new position of the loop has acceptable geometry for all of the residues (as evaluated by PROCHECK (40)). In the resulting model

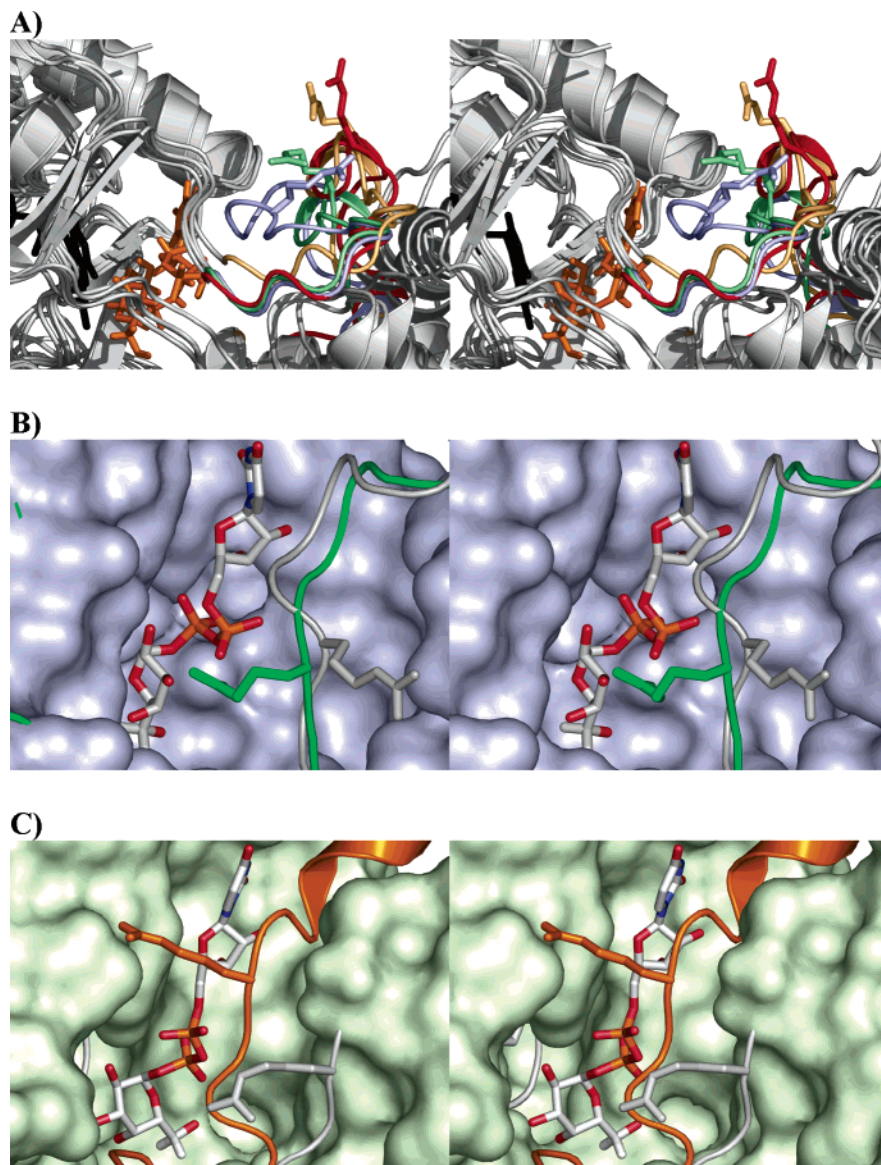


FIGURE 7: Role of mobile loop of UGM: Potential conformational change. (A) Ribbon depiction of the superposition of UGM from *E. coli*, *K. pneumoniae*, and *M. tuberculosis*. Monomers (A and B) from *E. coli* were superimposed along with those from *K. pneumoniae* and *M. tuberculosis* using LSQMAN (45). The cartoon representation UGM from all four monomers (monomers A and B from *E. coli* and a monomer from *K. pneumoniae*, and *M. tuberculosis*) are superimposed and shown in light gray. The residue corresponding to Arg170 in *E. coli* (Arg174 for *K. pneumoniae*) is shown in blue, green, red, and cream (for *E. coli* monomer A, B, *K. pneumoniae*, and *M. tuberculosis* UGM, respectively). The FAD from *E. coli* monomer A is shown in black. The modeled substrate (from monomer A derived model) is included and shown in orange. (B) Energy minimized model: *E. coli* UGM monomer A ("closed" conformation)—shown in surface representation, except for the loop (residues 157–185)—was used as the basis for an energy minimized model with Arg170 (shown in stick representation and colored gray) constrained to be 4 Å from the pyrophosphoryl group of UDP-Galp. The energy minimized model is shown in green, with Arg170 shown as a stick representation. The modeled UDP-Galp is shown as sticks, colored in CPK colors. (C) Model resulting from a molecular dynamics simulation of loop movement. Monomer B from *E. coli* ("open" conformation—shown in surface representation, as in (B)) was used as the starting point for a molecular dynamics simulation of possible loop movements. The UDP-Galp substrate was modeled in based on the positioning of the substrate relative to the FAD in monomer A. There were no constraints placed on any of the residues. The resulting model is colored orange.

(Figure 7B), the substrate binding affinity is 5 kcal/mol more favorable when Arg170 interacts with the phosphoryl group. That energy difference corresponds to a 4000-fold change in the binding constant. This value is consistent with previously reported studies of arginine–phosphate interactions (41). A 4000-fold alteration in the binding constant of UGM would be outside the range of the aforementioned fluorescence polarization assay.

To better understand the flexibility of this loop, we carried out a molecular dynamics simulation. The goal was to

evaluate how substrate binding might influence the movement of the loops. To simulate movements of the loop from the "open" conformation toward the putative "active" conformation, we modeled the proposed orientation of UDP-Galp (from monomer A (20)) into the monomer B structure (which adopts an "open" conformation (18)). A molecular dynamics simulation was then performed on this structure, with no distance constraints imposed. In the resulting model (Figure 7C), the flexible loop adopts a conformation similar to that seen in Figure 7B (when Arg170 is constrained to

contact the substrate). Similar results were obtained using the *K. pneumoniae* and *M. tuberculosis* structures (data not shown).

Implications from Analysis of Protein Variants of UGM. The results of the mutational study of the conserved residues of UGM support previously proposed mechanisms (19, 21). The substrate must be oriented so that it can interact with the FAD isoalloxazine ring. The reduced activity of the UGM variants lacking either of the two acidic residues suggests that these residues stabilize a positive charge, likely on the sugar moiety. The anionic nature of Glu301 is also conserved (e.g., some UGMs possess Asp residues at this position), suggesting that this residue stabilizes a positively charged intermediate. Substitution of Asp351 shows more significant effects on K_M than does substitution of Glu301, suggesting its role may be primarily hydrogen bond stabilization of the substrate.

A number of possibilities exist for the role of the two critical Arg residues. One potential role is in binding. Both of these residues (after loop movements) could engage in electrostatic interactions with the pyrophosphate moiety of the substrate. The results from fluorescence polarization and the energy minimization studies both support a dramatic (2–3 orders of magnitude) decrease in binding affinity when one of the residues is replaced. A decrease of approximately 10^6 in the binding constant as a result of the W160A mutation still resulted in detectable enzyme activity; therefore, the Arg substitution would have to afford a loss much greater than 10^6 in binding affinity. An alternative explanation is that the Arg residues engage in electrostatic interactions that stabilize the UDP as it serves as the leaving group. Loss of this stabilization could increase the required activation energy such that the barrier for isomerization cannot be overcome. Thus, the rate-limiting step of this reaction could be the breaking of the sugar phosphoryl bond and formation of the anionic UDP species. A third explanation is that the rearrangement of the mobile loop is required to form the active site and that substitution of either Arg residue prevents this conformational interconversion. This latter possibility is attractive given the STD-NMR data. Indeed, there are a number of aromatic residues present around the active site cleft of UGM, and the energy minimized model places two of these (Tyr185 and Phe186) within 4 Å of Arg174, raising the possibility of an arene–arginine interaction taking place (42, 43).

Our results are in general agreement with the model proposed by Yuan et al. (20), lending credence to the STD-NMR/docking approach for determining the binding modes for UDP-Galp and potential inhibitors. Still, we have identified Arg174 as having a key role in catalysis, yet Arg174 in the previous models points away from the active site cleft. A 3 Å movement of the C α backbone from the “closed” conformation and a 7 Å movement from the “open” conformation would position the guanidinium side chain such that it could interact with the pyrophosphoryl moiety. Our results indicate that the structures determined to date do not represent the active conformation. Accordingly, a structure with substrate or inhibitor will be illuminating. We anticipate that our results will provide a context for interpreting and analyzing future structural and biochemical experiments.

ACKNOWLEDGMENT

We are grateful to Dr. E. E. Carlson for the preparation of UDP-Galf. We thank the Saskatchewan Structural Sciences Centre for the expert help with the CD spectrophotometer.

REFERENCES

- Brennan, P. J., and Nikaido, H. (1995) The Envelope of Mycobacteria, *Annu. Rev. Biochem.* 64, 29–63.
- Knirel, Y. A., and Kochetkov, N. L. (1994) The Structure of Lipopolysaccharides of Gram-negative Bacteria. III. The Structure of O-antigens: A Review, *Biochemistry (Moscow)* 59, 1325–1383.
- Koplin, R., Brisson, J.-R., and Whitfield, C. (1997) UDP-Galactofuranose Precursor Required for Formation of the Lipopolysaccharide O Antigen of *Klebsiella pneumoniae* Serotype O1 Is Synthesized by the Product of the *rfbD*_{KPO1} Gene, *J. Biol. Chem.* 272, 4121–4128.
- Nassau, P. M., Martin, S. L., Brown, R. E., Weston, A., Monsey, D., McNeil, M. R., and Duncan, K. (1996) Galactofuranose Biosynthesis in *Escherichia coli* K-12: Identification and Cloning of UDP-Galactopyranose Mutase, *J. Bacteriol.* 178, 1047–1052.
- Stevenson, G., Neal, B., Liu, D., Hobbs, M., Packer, N. H., Batley, M., Redmond, J. W., Lindquist, L., and Reeves, P. (1994) Structure of the O-antigen of *Escherichia coli* K-12 and the Sequence of Its *rfb* Gene Cluster, *J. Bacteriol.* 176, 4144–4156.
- Barreto-Bergter, E. M., Travassos, L. R., and Gorin, P. A. J. (1980) Chemical Structure of the D-Galacto-D-Mannan Component From Hyphae of *Aspergillus niger* and Other *Aspergillus* spp, *Carbohydr. Res.* 86, 273–285.
- Bernard, M., and Latge, J.-P. (2001) *Aspergillus fumigatus* Cell Wall: Composition and Biosynthesis, *Med. Mycol.* 39 (Suppl. I), 9–17.
- Guest, G. M., and Momany, M. (2000) Analysis of Cell Wall Sugars in the Pathogen *Aspergillus fumigatus* and the Saprophyte *Aspergillus nidulans*, *Mycologia* 92, 1047–1050.
- de Lederkremer, R. M., and Colli, W. (1995) Galactofuranose-Containing Glycoconjugates in Trypanosomatids, *Glycobiology* 5, 547–552.
- Huang, C., and Turco, S. J. (1993) Defective Galactofuranose Addition in Lipophosphoglycan Biosynthesis in a Mutant of *Leishmania donovani*, *J. Biol. Chem.* 268, 24060–24066.
- Ilg, T., Etges, R., Overath, P., McConville, M. J., Thomas-Oates, J., Thomas, J., Homans, S. W., and Ferguson, M. A. (1992) Structure of *Leishmania mexicana* Lipophosphoglycan, *J. Biol. Chem.* 267, 6834–6840.
- McConville, M. J., Homans, S. W., Thomas-Oates, J. E., Dell, A., and Bacic, A. (1990) Structures of the Glycoinositolphospholipids from *Leishmania major*. A Family of Novel Galactofuranose-containing Glycolipids, *J. Biol. Chem.* 265, 7385–7394.
- McConville, M. J., Thomas-Oates, J. E., Ferguson, M. A. J., and Homans, S. W. (1990) Structure of the Lipophosphoglycan From *Leishmania major*, *J. Biol. Chem.* 265, 19611–19623.
- World Health Organization (2002) *Fact Sheet No. 104*, pp 1–230, The World Health Organization, Geneva.
- Pan, F., Jackson, M., Ma, Y., and McNeil, M. (2001) Cell Wall Core Galactofuran is Essential For Growth of Mycobacteria, *J. Bacteriol.* 183, 3991–3998.
- Scherman, M. S., Winams, K. A., Stern, R. J., Jones, V., Bertozzi, C. R., and McNeil, M. R. (2003) Drug Targeting *Mycobacterium tuberculosis* Cell Wall Synthesis: Development of a Microtiter Plate-Based Screen for UDP-Galactopyranose Mutase and Identification of an Inhibitor from a Uridine-Based Library, *Antimicrob. Agents Chemother.* 47, 378–382.
- Beis, K., Velupillai, S., Liu, H., Fullerton, S. W. B., Bamford, V. A., Sanders, D. A. R., Whitfield, C., McNeil, M. R., and Naismith, J. H. (2005) Crystal Structures of *Mycobacterium tuberculosis* and *Klebsiella pneumoniae* UDP-Galactopyranose Mutase in Oxidized State and *Klebsiella pneumoniae* UDP-Galactopyranose Mutase in the (Active) Reduced State, *J. Mol. Biol.* 348, 971–982.
- Sanders, D. A. R., Staines, A. G., McMahon, S. A., McNeil, M. R., Whitfield, C., and Naismith, J. H. (2001) UDP-Galactopyranose Mutase Has a Novel Structure and Mechanism, *Nat. Struct. Biol.* 8, 858–863.
- Fullerton, S. W. B., Daff, S., Sanders, D. A. R., Ingledew, W. J., Whitfield, S., Chapman, S. K., and Naismith, J. H. (2003)

- Potentiometric Analysis of UDP-Galactopyranose Mutase: Stabilization of the Flavosemiquinone by Substrate, *Biochemistry* 42, 2104–2109.
20. Yuan, Y., Wen, X., Sanders, D. A. R., and Pinto, B. M. (2005) Exploring the Binding Mechanism of UDP-Galactopyranose Mutase by STD-NMR Spectroscopy and Molecular Modeling, *Biochemistry* 44, 14080–14089.
 21. Soltero-Higgin, M., Carlson, E. E., Gruber, T. D., and Kiessling, L. L. (2004) A Unique Catalytic Mechanism for UDP-Galactopyranose Mutase, *Nat. Struct. Biol.* 11, 539–543.
 22. Zhang, Q., and Liu, H.-w. (2001) Mechanistic Investigation of UDP-Galactopyranose Mutase From *Escherichia coli* Using 2- and 3-Fluorinated UDP-Galactofuranose as Probes, *J. Am. Chem. Soc.* 123, 6756–6766.
 23. Huang, Z., Zhang, Q., and Liu, H. (2003) Reconstitution of UDP-Galactopyranose Mutase with 1-Deaza-FAD and 5-Deaza-FAD: Analysis and Mechanistic Implications, *Bioorg. Chem.* 31, 494–502.
 24. Caravano, A., Sinay, P., and Vincent, S. P. (2006) 1,4-Anhydrogalactopyranose Is Not an Intermediate of the Mutase Catalyzed UDP-Galactopyranose/Furanose Interconversion, *Bioorg. Med. Chem. Lett.* 16, 1123–1125.
 25. Sadeghi-Khomami, A., Blake, A. J., Wilson, C., and Thomas, N. R. (2005) Synthesis of a Carbasugar Analogue of a Putative Intermediate in the UDP-Galp-Mutase Catalyzed Isomerization, *Org. Lett.* 7, 4891–4894.
 26. Barlow, J. N., and Blanchard, J. S. (2000) Enzymatic Synthesis of UDP-(3-Deoxy-3-Fluoro)-D-Galactose and UDP-(2-Deoxy-2-Fluoro)-D-Galactose and Substrate Activity with UDP-Galactopyranose Mutase, *Carbohydr. Res.* 328, 473–480.
 27. Barlow, J. N., Girvin, M. E., and Blanchard, J. S. (1999) Positional Isotope Exchange Catalyzed by UDP-Galactopyranose Mutase, *J. Am. Chem. Soc.* 121, 6968–6969.
 28. Bradford, M. M. (1976) A Rapid and Sensitive Method For the Quantitation of Microgram Quantities of Protein Utilizing the Principle of Protein-Dye Binding, *Anal. Biochem.* 72, 248–254.
 29. Veerapen, N., Yuan, Y., Sanders, D. A. R., and Pinto, B. M. (2004) Synthesis of Novel Ammonium and Selenonium Ions and Their Evaluation as Inhibitors of UDP-Galactopyranose Mutase, *Carbohydr. Res.* 339, 2205–2217.
 30. Marlow, A. L., and Kiessling, L. L. (2001) Improved Chemical Synthesis of UDP-Galactofuranose, *Org. Lett.* 3, 2517–2519.
 31. Zhang, Q., and Liu, H.-w. (2000) Studies of UDP-Galactopyranose Mutase from *Escherichia coli*: An Unusual Role of Reduced FAD in Its Catalysis, *J. Am. Chem. Soc.* 122, 9065–9070.
 32. Soltero-Higgin, M., Carlson, E. E., Phillips, J. H., and Kiessling, L. L. (2004) Identification of Inhibitors for UDP-Galactopyranose Mutase, *J. Am. Chem. Soc.* 126, 10532–10533.
 33. Morris, G. M., Goodsell, D. S., Halliday, R. S., Huey, R., Hart, W. E., Belew, R. K., and Olson, A. J. (1998) Automated Docking Using a Lamarckian Genetic Algorithm and an Empirical Binding Free Energy Function, *J. Comput. Chem.* 19, 1639–1662.
 34. Notredame, C., Higgins, D. G., and Heringa, J. (2000) T-Coffee: A Novel Method For Fast and Accurate Multiple Sequence Alignment, *J. Mol. Biol.* 302, 205–217.
 35. Barlow, J. N., Marcinkeviciene, J., and Blanchard, J. S. (1999) The Enzymatic Conversion of UDP-Galactopyranose to UDP-Galactofuranose, in *Enzymatic Mechanisms* (Frey, P. A., and Northrop, D. B., Eds.) pp 98, IOS Press, Burke, VA.
 36. Caravano, A., Mengin-Lecreulx, D., Brondello, J.-M., Vincent, S. P., and Sinjay, P. (2003) Synthesis and Inhibition Properties of Conformational Probes for the Mutase-Catalyzed UDP-Galactopyranose/Furanose Interconversion, *Chem. Eur. J.* 9, 5888–5898.
 37. Weiss, W. I., and Drickamer, K. (1996) Structural Basis of Lectin-Carbohydrate Recognition, *Annu. Rev. Biochem.* 65, 441–473.
 38. Quiocho, F. A. (1986) Carbohydrate-Binding Proteins: Tertiary Structures and Protein-Sugar Interactions, *Annu. Rev. Biochem.* 55, 287–315.
 39. Carlson, E. E., May, J. F., and Kiessling, L. L. (2006) Chemical Probes of UDP-Galactopyranose Mutase, *Chem. Biol.* 13, 825–837.
 40. Laskowski, R. A., MacArthur, M. W., Mooss, D. S., and Thornton, J. M. (1993) PROCHECK: A Program to Check the Stereochemical Quality of Protein Structures, *J. Appl. Crystallogr.* 26, 283–291.
 41. de la Mata, I., Garica, J. L., Gonzalez, C., Menendez, M., Canada, J., Jimenez-Barbero, J., and Asensio, J. L. (2002) The Impact of R53C Mutation on the Three-Dimensional Structure, Stability and DNA-Binding Properties of the Human Hsx-1 Hoemodomain, *ChemBioChem* 3, 726–740.
 42. Sörme, P., Arnoux, P., Kahl-Knutsson, B., Leffler, H., Rini, J. M., and Nilsson, U. J. (2005) Structural and Thermodynamic Studies on Cation- π Interactions in Lectin-Ligand Complexes: High-Affinity Galectin-3 Inhibitors Through Fine-Tuning of an Arginine-Arene Interaction, *J. Am. Chem. Soc.* 127, 1737–1743.
 43. Sörme, P., Qian, Y., Nyholm, P.-G., Leffler, H., and Nilsson, U. J. (2002) Low Micromolar Inhibitors of Galectin-3 Based on 3'-Derivatization of *N*-Acetyllactosamine, *ChemBioChem* 3, 183–189.
 44. Gouet, P., Courcelle, E., Stuart, D. I., and Metz, F. (1999) ESPript: Analysis of Multiple Sequence Alignments in PostScript, *Bioinformatics* 15, 305–308.
 45. Kleywegt, G. J., and Jones, T. A. (1997) Detecting Folding Motifs and Similarities in Protein Structures, *Methods Enzymol.* 277, 525–545.

BI7002795